

Dwarf-Dwarf Interactions Can Both Trigger and Quench Star Formation

ERIN KADO-FONG,¹ AZIA ROBINSON,² KRISTINA NYLAND,³ JENNY E. GREENE,² KATHERINE A. SUESS,^{4,*}
SABRINA STIERWALT,⁵ AND RACHAEL BEATON^{6,7}

¹*Physics Department, Yale Center for Astronomy & Astrophysics, PO Box 208120, New Haven, CT 06520, USA*

²*Department of Astrophysical Sciences, Princeton University, Princeton, NJ 08540, USA*

³*U.S. Naval Research Laboratory, 4555 Overlook Ave SW, Washington, DC 20375, USA*

⁴*Kavli Institute for Particle Astrophysics and Cosmology and Department of Physics, Stanford University, Stanford, CA 94305, USA*

⁵*Physics Department, 1600 Campus Road, Occidental College, Los Angeles, CA 90041, USA*

⁶*Space Telescope Science Institute, Baltimore, MD 21218, USA*

⁷*Department of Physics and Astronomy, Johns Hopkins University, Baltimore, MD 21218, USA*

ABSTRACT

It is exceedingly rare to find quiescent low-mass galaxies in the field at low redshift. UGC5205 is an example of such a quenched field dwarf ($M_{\star} \sim 3 \times 10^8 M_{\odot}$). Despite a wealth of cold gas ($M_{\text{HI}} \sim 3.5 \times 10^8 M_{\odot}$) and ultraviolet emission that indicates significant star formation in the past few hundred Myr, there is no detection of H α emission – star formation in the last ~ 10 Myr – across the face of the galaxy. Meanwhile, the near equal-mass companion of UGC5205, PGC027864, is starbursting ($\text{EW}_{\text{H}\alpha} > 1000 \text{ \AA}$). In this work, we present new Karl G. Jansky Very Large Array (VLA) 21 cm line observations of UGC5205 showing that the lack of star formation is caused by an absence of HI in the main body of the galaxy. The HI of UGC5205 is highly disturbed; the bulk of the HI resides in several kpc-long tails, while the HI of PGC027864 is dominated by ordered rotation. We model the stellar populations of UGC5205 to show that, as indicated by the UV-H α emission, the galaxy underwent a coordinated quenching event $\sim 100 - 300$ Myr ago. The asymmetry of outcomes for UGC5205 and PGC027864 demonstrate that major mergers can both quench *and* trigger star formation in dwarfs. However, because the gas remains bound to the system, we suggest that such mergers only temporarily quench star formation. We estimate a total quenched time of ~ 560 Myr for UGC5205, consistent with established upper limits on the quenched fraction of a few percent for dwarfs in the field.

1. INTRODUCTION

Dwarf galaxies ($M_{\star} < 10^9 M_{\odot}$) provide a crucial laboratory for the processes, both internal and environmental, that regulate star-formation. Unlike more massive galaxies, empirical evidence suggests that low-mass galaxies are nearly always star-forming in the field, with less than 1% of galaxies at $M_{\star} = 10^8 M_{\odot}$ expected to be quenched outside the influence of a massive galaxy (Geha et al. 2012). While merging and feedback are actively discussed as mechanisms for truncating star formation in massive galaxies (e.g., Blanton & Moustakas 2009), the dearth of a build-up of quenched dwarfs in the field suggests that these mechanisms either do not

exist in the dwarf regime, or are inefficient at quenching dwarf galaxies.

In this paper, we study an intriguing exception that may prove the rule. UGC5205 is a dwarf galaxy ($M_{\star} = 3 \times 10^8 M_{\odot}$) at $d \approx 21$ Mpc that is classified as a field dwarf by standard criteria (Geha et al. 2012). However, UGC5205 is in an interacting pair with the comparable-mass galaxy PGC027864. This pair is part of the TiNy Titans survey of dwarf interacting pairs (Stierwalt et al. 2015, 2017). While both galaxies are very HI rich, there is no sign of H α emission across the face of UGC5205 (Pracy et al. 2012). PGC027864, meanwhile, is vigorously star-forming, and has been studied in the UV as a local analog to high redshift galaxies (e.g., Izotov & Thuan 2016; Senchyna et al. 2022). The two galaxies in this pair thus have radically different effective star formation efficiencies (where we will roughly define star formation efficiency as $\text{SFE} = \text{SFR}/M_{\text{HI}}$) despite very

Corresponding author: Erin Kado-Fong
erin.kado-fong@yale.edu

* NHFP Hubble Fellow

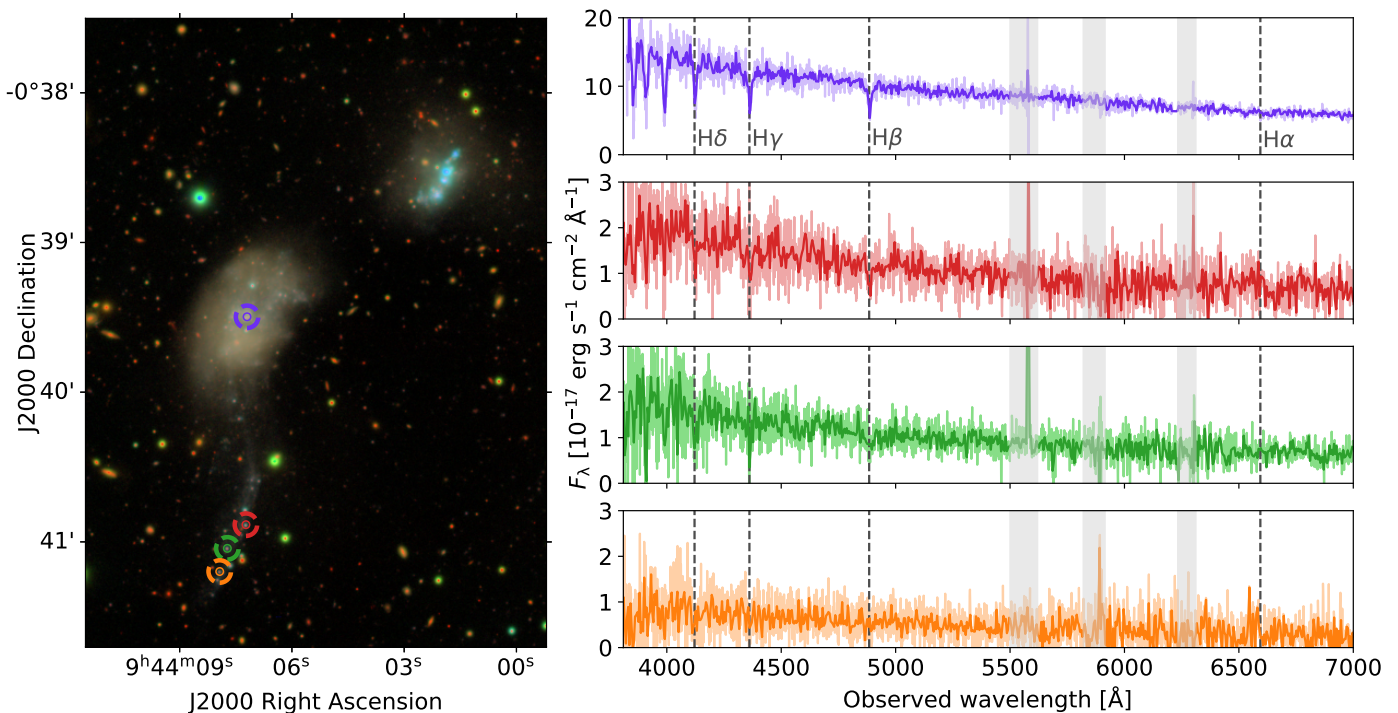


Figure 1. *Left:* HSC-SSP *gri* composite image of UGC5205 (southeast) and PGC027864 (northwest). The locations of the four archival SDSS spectra are shown in orange, green, red, and purple. The inner circles show the extent of the SDSS fiber 3'' diameter. *Right:* the archival SDSS spectra (same colors as at left). We show the unbinned spectra as light curves and the spectra binned to $\Delta\lambda = 5 \text{ \AA}$ as bold curves. Grey shaded patches show regions with under-subtracted sky lines. The blue dashed lines show the Balmer series redshifted to $z = 0.00496$; there are no significant emission lines in the spectra of UGC5205.

similar stellar masses, HI masses, and large scale environments.

Our aim in the present work is to understand the root of this apparent disparity in SFE by studying the morphology and kinematics of the HI gas, particularly in the quenched dwarf UGC5205. While mergers are a recognized mechanism for quenching star formation in massive galaxies (see, e.g. Hopkins et al. 2008; Somerville et al. 2008; Quai et al. 2021), this pathway has not been explored as a quenching mechanism for dwarfs. In fact, although signatures of dwarf-dwarf interactions and mergers at this mass ratio are observed in a few percent of dwarfs (Stierwalt et al. 2015; Besla et al. 2018; Kado-Fong et al. 2020), for both dwarf pairs (Stierwalt et al. 2015) and post-coalescence mergers (Kado-Fong et al. 2020), dwarf-dwarf interactions appear to trigger, rather than quench, star formation. In particular, long-term quenching via low-mass mergers is disfavored due to the lack of an emergent field dwarf population at low redshift (Geha et al. 2012) despite theoretical expectations that major mergers between dwarfs are relatively common ($\sim 10\%$) since $z \sim 1$ and direct evidence for major mergers at low- z (see, e.g. Stierwalt et al. 2015;

Kado-Fong et al. 2020). UGC5205 thus provides an excellent laboratory to interrogate the physical processes at play during dwarf-dwarf mergers, and how quenching can occur dynamically in such a gas-rich system.

This manuscript is structured as follows. Section 2 introduces the Karl G. Jansky Very Large Array (VLA) data that we obtained of UGC5205 and PGC027864, while Section 3 discusses the analysis of the VLA data and archival UV-optical datasets. Finally, in Section 4 we discuss the viability of proposed mechanisms to quench UGC5205 as well as the implications that the existence of UGC5205 has on the existence and evolution of a quiescent dwarf population.

Throughout this analysis, we adopt a flat Λ CDM cosmology with $\Omega_m = 0.3$ ($\Omega_\Lambda = 0.7$), and $H_0 = 70 \text{ km s}^{-1} \text{ Mpc}^{-1}$.

2. OBSERVATIONS AND DATA REDUCTION

In this section we present and discuss new multi-configuration VLA observations from project 21A-081. We observed UGC5205 in the L-band centered at 1413.8929 MHz in the D configuration on March 25, 2021 for 2 hr (1.5 hr on source). On June 13 and 15, 2021 we observed UGC5205 with an identical frequency

tuning in the C configuration for 3.5 hr (2.5 hr on source) each, for a total of 5 hr on source. Phase referencing using the calibrator J0943-0819 was performed every three minutes. Once per observation, we performed flux density and bandpass calibration using the calibrator 3C138 for five minutes.

Initial flagging, flux density scaling, and calibration for the three measurement sets were performed with the Common Astronomy Software Applications (CASA; CASA Team et al. 2022) pipeline version 1.4.2¹, with additional flagging, data reduction, and imaging performed with CASA version 6.4.3.27. We reduced each of the two C configuration scheduling blocks separately; we combined the reduced datasets from each block as the final step to produce the final C configuration dataset. We note that the C configuration data contained severe radio frequency interference (RFI) requiring manual flagging using the PLOTMS and FLAGDATA tasks.

For each configuration, we used the task TCLEAN to produce an initial image cube containing both the line and continuum emission. We imaged the data with a spectral resolution of 6.6 km/s and chose ‘Briggs’ weighting with a robust parameter of 0.3 to achieve an optimal compromise among sensitivity, angular resolution, and sidelobe suppression. The cell sizes used for imaging the C and D configuration datasets were 2.2 and 9 arcseconds, respectively. The HI emission associated with UGC5205 and MGC+00-25-010 spanned channels 224 to 252 (1575 km/s to 1395 km/s). We performed continuum subtraction using the CASA task UVCONTSUB before producing the final image cube for each configuration with TCLEAN. Our final C configuration image achieved an rms noise of 7.6 mJy beam⁻¹ and our final D configuration image reached an rms of 1.5 mJy beam⁻¹.

In the subsequent sections, we will consider the VLA data coincident with UGC5205 and with PGC027864 separately (in Section 3.2 and Section 3.3, respectively). For the reader’s convenience, however, we tabulate key VLA figures here. The C-array moment zero map of the system is shown in Figure 2, while the C-array moment one map of the system is shown in Figure 3. The moment zero map of the D-array data is shown in Figure 13. Channel maps of UGC5205 and PGC027864 are shown separately in Figure 5 and Figure 6, respectively.

3. RESULTS

3.1. Optical Morphology

Before presenting the spatially resolved HI data obtained with VLA, we will briefly detail the optical morphology of the galaxy pair in order to provide context to the reader in interpreting the gas reservoirs of these two galaxies.

In Figure 1, we show an image from the HyperSuprime Camera data of the UGC5205/PGC027864 pair in the *gri*-bands. Superposed on the image are the locations of the four SDSS fibers that took the spectra shown on the right-hand side. We point out a few key features of this interacting system. First, there is clearly a tidal feature stretching to the South of UGC5205. Likely this tail is associated with the ongoing interaction with PGC027864 to the North. The striking point, and the reason for our focus on UGC5205, is that despite the clear evidence of young stellar ages in the spectra (a point to which we will return more quantitatively in Section 3.5), there is no H α detected at any position covered by the SDSS. Likewise an integral-field observation of the galaxy center shows no H α emission (Pracy et al. 2012).

In contrast, as is clear from this three-color image, PGC027864 is star-bursting. The low metallicity and high star formation rate of this galaxy have been documented extensively (e.g., Shirazi & Brinchmann 2012; Senchyna et al. 2017).

Having addressed the optical morphology, we can now consider the spatially resolved HI data for this galaxy pair. The moment 0 maps of the C-array VLA data are shown as contours overlaid on the HSC-SSP optical imaging of UGC5205 and PGC027864 in Figure 2. We see immediately see that the HI associated with UGC5205 has a complex morphology and the HI associated with PGC027864 is relatively less disturbed.

3.2. HI morphology and kinematics of UGC5205

There are three primary components of the HI associated with UGC5205 that we will consider throughout the paper, as labeled in Figure 2. While there appears to be gas to the southeast of the galaxy (components B1 & B2) and gas to the northwest of the galaxy (component A), there is no detected concentration of HI in the galaxy center.

To better understand the nature of the complex HI morphology of UGC5205, we show the first moment maps in Figure 3. Here, the left panel shows the full extent of the HI associated with UGC5205 and PGC027864, while the right top and bottom panels show the difference in velocity from the peak heliocentric velocity of the HI profile of UGC5205 and PGC027864, respectively.

¹ <https://science.nrao.edu/facilities/vla/data-processing/pipeline/scripted-pipeline>

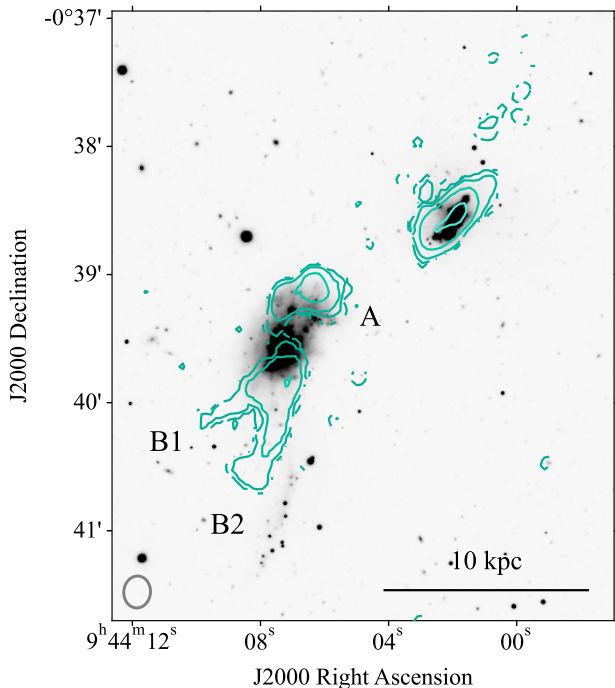


Figure 2. The moment 0 map of the VLA C-array data (green contours), overlaid over the HSC-SSP g-band optical image. Significant HI gas is found coincident with both UGC5205 (southeast) and PGC027864 (northwest). We find that the gas associated with UGC5205 is morphologically complex, with three clear tails (labels A, B1, and B2) visible in the VLA data. The gas associated with PGC027864 is notably less disturbed, though there is significant emission from a disturbed component to the northwest. We show contours with a constant logarithmic offset beginning from $\Sigma_{\text{HI}} = 10^5 M_{\odot} \text{ beam}^{-1}$ (or an HI column density of $N(\text{HI}) = 5.4 \times 10^{18} \text{ cm}^{-2}$).

From the moment 1 maps, we note the varied velocities along B1 and B2. The systemic velocity of the stars, as measured from the absorption features in the SDSS spectra, is $1500 \pm 18 \text{ km s}^{-1}$. Nearly all of the gas is redshifted relative to this velocity, with only the very tip of tail B2 overlapping in velocity with the galaxy systemic velocity. This velocity mismatch was previously established by single-dish spectra (see Section B.1). Tail B1 and component A share a similar velocity of $1500\text{--}1550 \text{ km s}^{-1}$, and there is a small gradient across component A.

B2 extends away from the galaxy center in a similar direction as the stellar tidal feature. Because of the spatial proximity to the stellar tidal feature, and due to the narrow range of velocities we see in B1 and B2 in the moment 1 map, we suggest that B1 and B2 are tidal

Table 1. HI masses associated with each component of UGC5205.

Galaxy	Component	Velocity	Channel	M_{HI}^a
		km s^{-1}		$10^8 M_{\odot}$
UGC5205	<i>total</i>	1575 – 1507	224–234	3.47
	A	1575–1507	...	1.33
	B1	1547–1500	228–235	1.41
	B2	1575–1547	224–228	...
PGC027864	<i>total</i>	1481 – 1400	238–250	2.11

^aMasses are calculated at the luminosity distance of the systemic optical velocity of UGC5205.

in nature. We show the channel maps of UGC5205 in Figure 5 – B1 and B2 span only a couple of channels, and we see little to no gradient along the features. Both B1 and B2 are redshifted relative to UGC5205, but their velocity structure seems quite typical for tidal tails.

The nature of Feature A, which sits between the two galaxies spatially but is much closer to the systemic velocity of UGC5205, is unclear. The total mass of HI associated with UGC5205 is $3.47 \times 10^8 M_{\odot}$. The mass in HI associated with the extended features is split almost equally between A and B1+B2. Specifically, as detailed in Table 1, component A has an HI mass of $1.33 \times 10^8 M_{\odot}$ while the two tails have a combined mass of $1.41 \times 10^8 M_{\odot}$. The apertures used to measure the enclosed HI mass in each component are shown as dashed ellipses in Figure 4.

Component A spans a range of velocities ($1520 \lesssim v \lesssim 1570 \text{ km s}^{-1}$). There is some evidence for a velocity gradient across Component A, with the material to the East falling at higher velocity and the material to the West (closest to the companion galaxy) at the lowest velocity, as can be seen directly from the channel maps in Figure 5. Component A, recall, comprises roughly 50% of the total HI associated with UGC5205.

The overall morphological and kinematic picture of UGC5205 as unveiled by the VLA data reveals a highly disturbed gas reservoir. It is striking to note that the HI is systematically redshifted with respect to the systemic velocity of UGC5205 and that there is a strong dearth of HI in the center of the galaxy. Although a full suite of matched simulations is beyond the scope of this work, the asymmetry of the system in velocity space argues against a scenario in which the gas morphology results from purely secular effects – again pointing to a tidal origin of the gas tails around UGC5205.

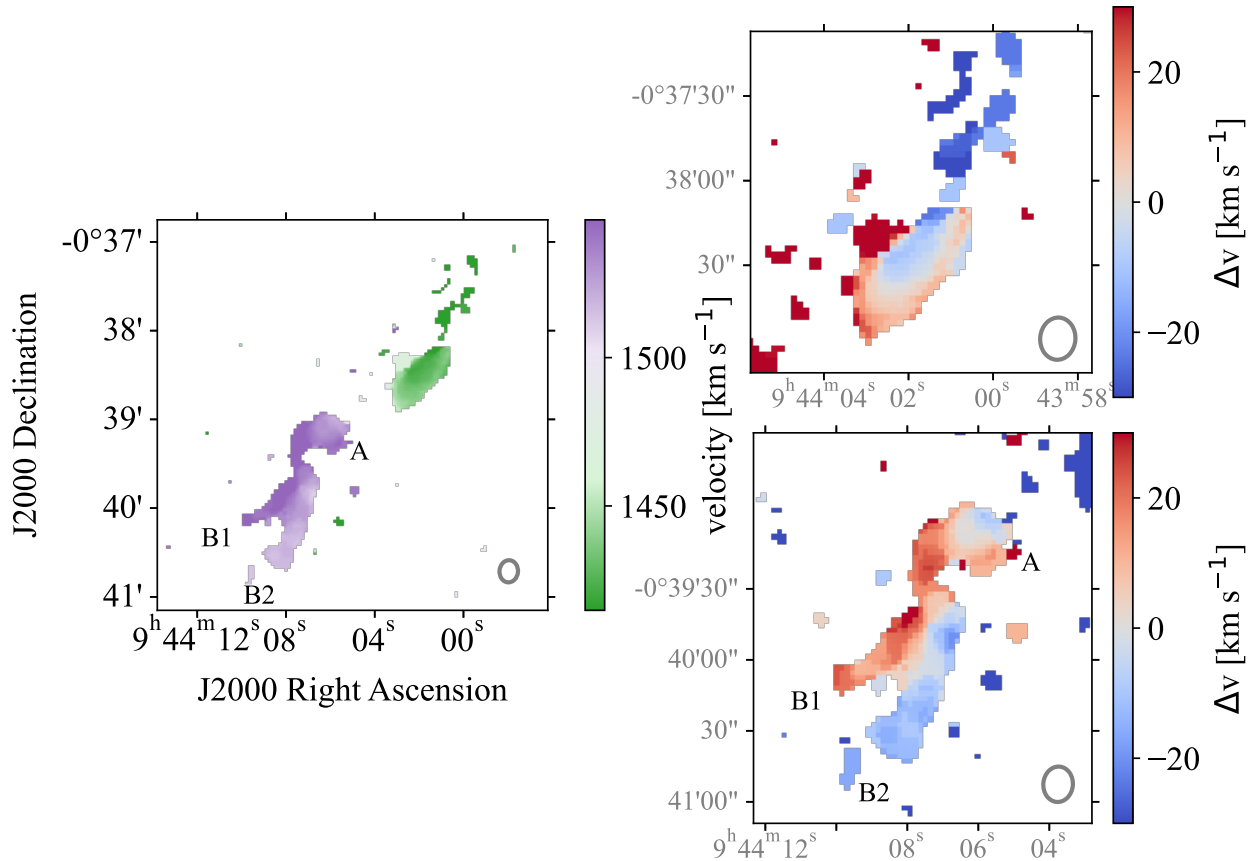


Figure 3. The first moment map of UGC5205 and PGC027864. At left we show the full moment map, while at right we show a portion of the map over a smaller spatial and velocity range. In each panel, the average C-array beam is shown in the bottom right corner. We find that the HI associated with UGC5205 and that associated with PGC027864 are systematically offset in velocity. The gas associated with UGC5205 is highly disturbed, with extended features A, B1, & B2 (as labeled) showing evidence of an offset in mean velocity. Though there is some blueshifted emission of the gas associated with PGC027864, the majority of the emission is consistent with ordered rotation.

Finally, we note that given the velocity difference (with respect to the stellar systemic velocity) and extent of the tidal features, and the expected total mass of the dwarf pair, the HI of UGC5205 should remain bound to UGC5205 and/or the eventual product of the merger between UGC5205 and PGC027864.

3.3. HI morphology and kinematics of PGC027864

In contrast to the complex morphology and kinematics of UGC5205, the HI reservoir of PGC027864 is relatively undisturbed. The systemic velocity of PGC027864 is 1640 km s^{-1} (see Table 2), as measured from the SDSS spectra. Unlike UGC5205, the HI peak velocity is well-aligned with the optical emission lines of PGC027864.

In Figure 6 we present the channel maps for PGC027864. As is implied in Figure 3, we see a gra-

dient in velocity, with the lowest-velocity gas arising from the North-west component of the galaxy (at $\sim 1400 \text{ km s}^{-1}$), and the highest-velocity gas arising from the Southeast (at $\sim 1470 \text{ km s}^{-1}$). The channel maps of PGC027864 show evidence for significant non-rotational motion, with emission in the southeast extending over a range of $v_{\text{los}} \sim 70 \text{ km s}^{-1}$.

We also see evidence for a more regular rotation curve across the face of this galaxy, though as noted above there is significant evidence for disturbance. We estimate the rotational velocity of PGC027864 in two ways: by constructing an integrated spectrum of the HI associated with PGC027864 and measuring W_{50} , the full width at half beam power, and using the 3D tilted ring fitter ${}^{\text{3D}}\text{Barolo}$, which is well-suited to low resolution kinematic analysis (Di Teodoro & Fraternali 2015), to

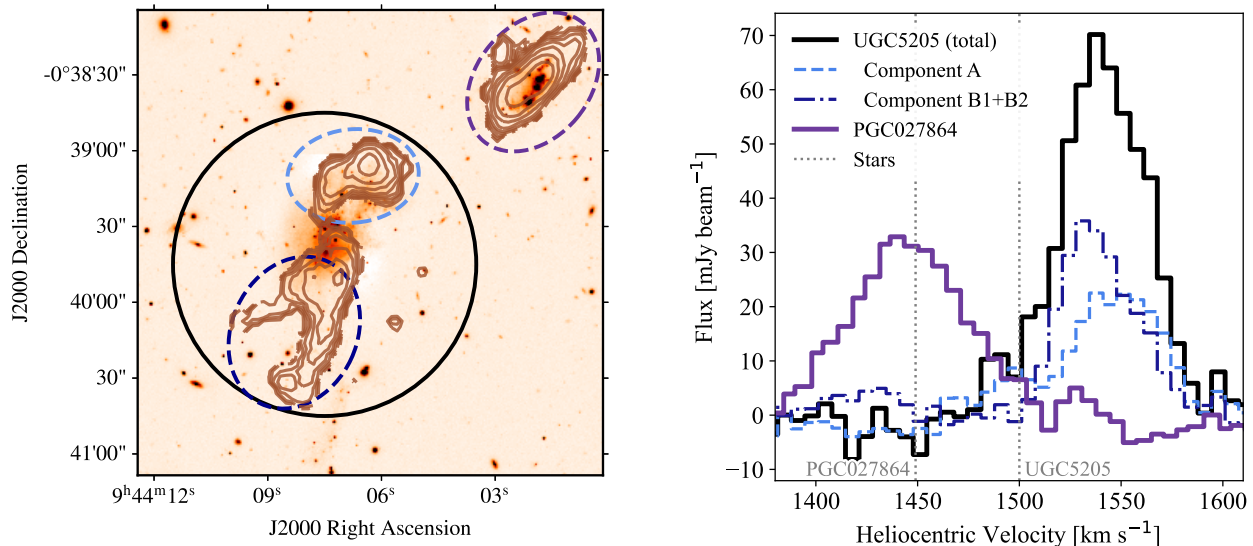


Figure 4. Integrated spectra of each component of the HI emission associated with UGC5205 and PGC027864. Each ellipse at left indicates an extraction region corresponding to an integrated spectrum at right as indicated by color; note that in this figure, component A is encompassed by the “head” extraction region while both components B1 and B2 are within the “Tail” extraction region. All spectra have been extracted using CASA IMVIEW. The grey dashed vertical line shows the systemic optical velocity of UGC5205.

fit a rotation curve (and thus an associated v_{rot}) to the VLA cube localized around PGC027864. We fix the inclination to $i = 54$ deg following the published inclination from the HyperLEDA database. Following Ponomareva et al. (2021), for a well-ordered rotating disc galaxy these two quantities should be related as $2v_{\text{rot}} \approx W_{50}$.

Our best-fitting 3^{D} Barolo model is shown in Figure 7. We find an average $v_{\text{rot}} = 28 \pm 5$ km s $^{-1}$, though we find that there is significant structure to the velocity map of PGC027864 that is not well-fit by the tilted ring model. This is not surprising given that there is significant 21cm emission by HI that has been stripped from the main body of the galaxy, as shown in Figure 2. When we construct an integrated spectrum containing all 21cm emission associated with PGC027864, we measure $W_{50} = 73 \pm 3$ km s $^{-1}$, somewhat higher than the expected $W_{50} = 2v_{\text{rot}}$ expectation. When we exclude the emission from HI that is spatially offset from the main body of PGC027864, we find $W_{50} = 62 \pm 2$ km s $^{-1}$, in good agreement with the v_{rot} measurement from 3^{D} Barolo.

Given these kinematic measures of the HI associated with PGC027864, we can attempt to place the galaxy on the baryonic Tully-Fisher relation (Ponomareva et al. 2021). We caution that we expect that both kinematic measures will be biased somewhat high given that the gas of PGC027864 shows evidence of disturbance. We

estimate the total baryonic mass of PGC027864 as

$$\begin{aligned} M_{\text{bar}} &= 1.4M_{\text{HI}} + M_{\star} \\ &= 3.6 \times 10^8 M_{\odot}, \end{aligned} \quad (1)$$

where the multiplicative factor of 1.4 is a correction for the mass in Helium and heavier elements. We ignore the mass contribution of H_2 both because the gas reservoir is expected to be dominated by HI at these stellar masses, with H_2 contributing $M_{\text{H}_2}/(M_{\text{HI}} + M_{\text{H}_2}) \lesssim 0.2$ (Leroy et al. 2008; Kado-Fong et al. 2022b), and to follow literature norms. In particular, from the measured baryonic Tully-Fisher relation (bTFR) of Ponomareva et al. (2021), which traces the correlation between total baryonic mass and galaxy rotational velocity, we expect a baryonic mass of $M_{\text{bar}} = 1.4_{-0.9}^{+2.2} \times 10^8 M_{\odot}$, where the uncertainty reflects both the uncertainty of the inferred velocity and the scatter in the bTFR. PGC027864 therefore lies within one sigma of the measured bTFR, which is consistent with the interpretation that ordered rotation dominates the HI velocity field.

3.4. Integrated Star Formation Rates: $\text{H}\alpha$ and UV Estimates

Although UGC5205 shows no sign of $\text{H}\alpha$ emission across its face, it is well-detected in the UV. The differing timescales over which $\text{H}\alpha$ and UV emission trace star formation can therefore give us insight into the recent star formation history of UGC5205 and PGC027864.

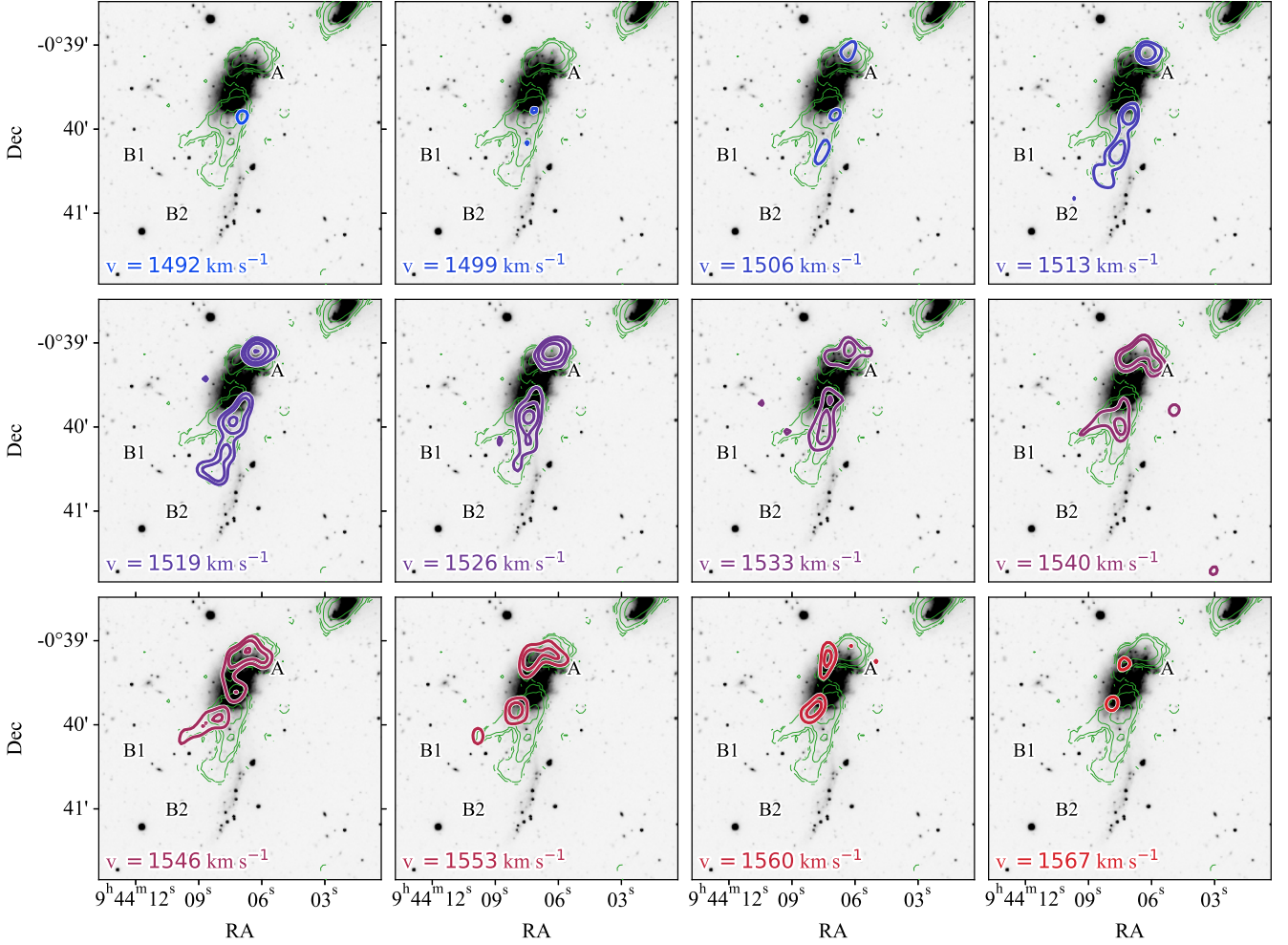


Figure 5. Channel maps for channels where significant 21cm line emission is detected around UGC5205. As a visual guide, the tidal components of UGC5205 (A, B1, and B2) labeled and the moment 0 H I map are shown as green contours in each panel. The narrow width of the H I components A, B1, and B2 in velocity space support the interpretation that these features are tidal in nature. The contours of the channel maps begin at 3 times the RMS of the C-array data (0.76 mJy/beam) and increase by a factor of 2^n at the n^{th} contour.

We estimate the integrated star formation rate across the main bodies of UGC5205 and PGC027864 from both GALEX UV photometry and the SDSS $H\alpha$ emission – or, in the case of UGC5205, an upper limit thereof. To prevent systematic offsets between the UV and $H\alpha$ -derived star formation rates, we compute the L_{UV} -SFR and $L_{H\alpha}$ -SFR relations using the python implementation `pythonfspi` of the Flexible Stellar Population Synthesis (fspi, Conroy & Gunn 2010) framework assuming the Binary Population and Spectral Synthesis (BPASS Eldridge & Stanway 2016) stellar isochrone library and a Kroupa initial mass function (IMF) (Kroupa 2001). We assume that the star formation rate has been constant for the past 10 Myr to compute $L_{H\alpha}$ and constant for the past 300 Myr to compute L_{UV} . This yields a

conversion of:

$$\frac{\text{SFR}(H\alpha)}{[M_{\odot} \text{ yr}^{-1}]} = 5.03 \times 10^{-42} \frac{L_{H\alpha}}{[\text{erg s}^{-1}]} \quad (2a)$$

$$\frac{\text{SFR}(FUV)}{[M_{\odot} \text{ yr}^{-1}]} = 1.06 \times 10^{-28} \frac{L_{FUV}}{[\text{erg s}^{-1} \text{ Hz}^{-1}]} \quad (2b)$$

These calibrations differ significantly from the Kennicutt (1998) conversions as published, but are within 5% and 25% of the conversions when the difference between the chosen IMF is taken into account.

We use imaging from the GALEX Medium Imaging Survey (MIS)² to measure FUV and NUV fluxes in the

² The GALEX observations used in this work can be found in the Mikulski Archive for Space Telescopes (MAST) via [10.17909/qj70-dv28](https://archive.stsci.edu/missions/galex/).

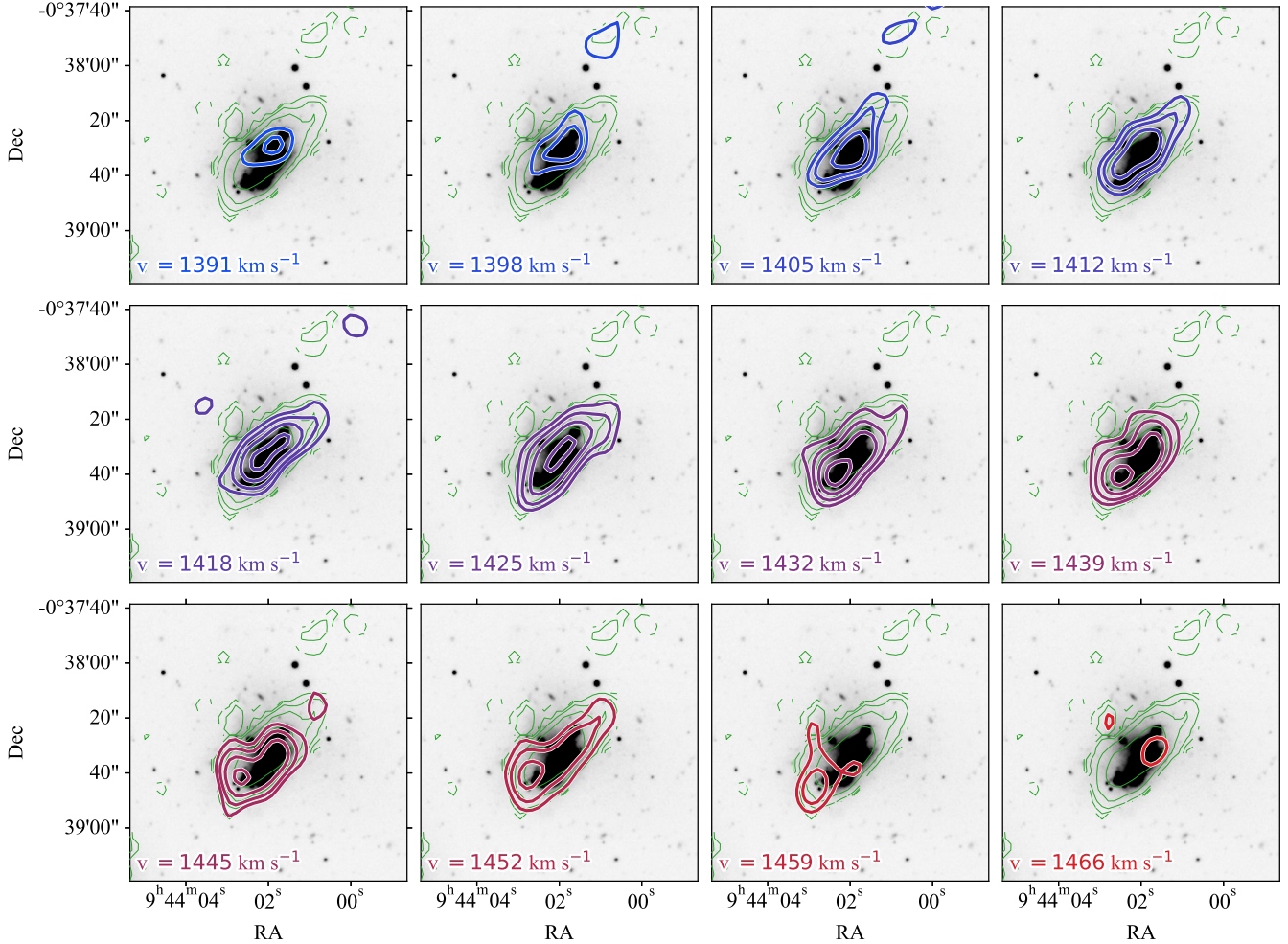


Figure 6. The same as Figure 5, but for channels with significant emission around PGC027864. There is evidence for disturbance in the HI profile of PGC027864 at $1391 \leq v \leq 1405 \text{ km s}^{-1}$, but the bulk of the HI associated with PGC027864 appears consistent with ordered rotation (as corroborated in Figure 7).

main bodies of UGC5205 and PGC027864, where we determine the geometry of the elliptical aperture³ using `sep`, a python implementation of the SExtractor object segmentation algorithm (Bertin & Arnouts 1996). Galactic extinction in both bands is corrected for using the Schlafly & Finkbeiner (2011) galactic reddening measurements⁴.

The estimation of an $H\alpha$ -based star formation rate is straightforward for PGC027864 and somewhat less so for UGC5205, given the lack of $H\alpha$ across the main body of the galaxy.

³ We set the limit of the aperture to $R = 3$, in accordance with the approximate isophotal limit where the ellipse is defined as $CXX\Delta x^2 + CYY\Delta y^2 + CXY\Delta x\Delta y = R^2$ using the standard definition of the SExtractor geometric parameters set forth in (Bertin & Arnouts 1996)

⁴ Obtained via the IRSA Galactic Dust Reddening and Extinction database: [10.26131/IRSA537](https://irsa.ipac.caltech.edu/data/DR16/galactic/)

We measure $EW_{H\alpha,em}$ of PGC027864 from its galactic extinction-corrected SDSS spectrum, where we fit the $H\alpha$, $[N II]\lambda 6548\text{\AA}$, and $[N II]\lambda 6583\text{\AA}$ lines simultaneously as equal-width Gaussians with a scalar continuum. We additionally fit $H\beta$ in order to correct for internal reddening via the Balmer decrement.

Let us now consider an upper limit for the equivalent width of the $H\alpha$ emission in the main body of UGC5205. Integral Field Unit (IFU) spectroscopy from the Wide Field Spectrograph (WiFeS) did not detect $H\alpha$ emission across the main body of UGC5205 (Pracy et al. 2012). The strong Balmer absorption lines in the blue imply an upper limit of $EW_{H\alpha} < 5\text{\AA}$ across the main body of UGC5205 after stellar absorption corrections, but neither emission nor absorption were detected at the expected observed wavelength of $H\alpha$. We can therefore only place an upper limit on the $H\alpha$ -based SFR of UGC5205. To be consistent with the $H\alpha$ -based SFR we will estimate for PGC027864, we use the central SDSS

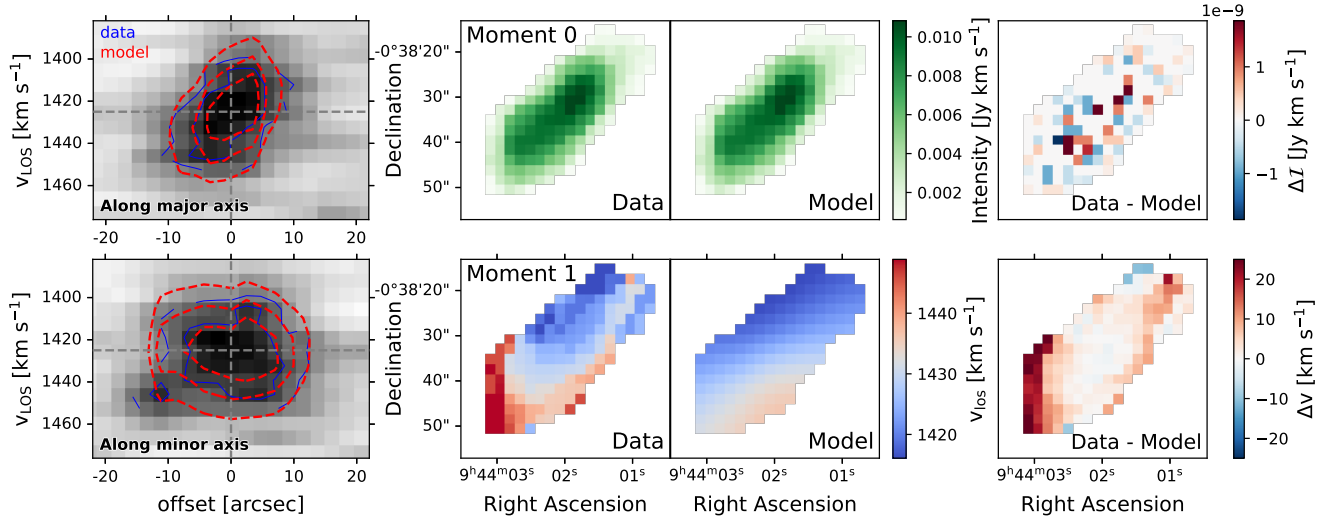


Figure 7. The best-fit 3D tilted ring model of 3^{D} Barolo for PGC027864. In the left column we show the PV diagram along the major (top) and minor (bottom) axes. The data are shown in greyscale with the model (red) and analogous data (blue) contours overlaid at the same levels. Grey dashed lines mark the spatial center and systemic velocity of the system. The middle set of panels show the real (left) and model (right) first (top row) and second moment maps (bottom row) as calculated by 3^{D} Barolo. The right column shows the difference between the real and model moment maps. Although the tilted ring model can describe the bulk rotational motion in the main body of PGC027864, it does not reproduce the redshifted material in the southeast region of PGC027864. We suggest that this material is the receding component of a stripped gas tail that can be seen as blueshifted material to the northwest in the bottom right panel of Figure 3.

spectrum of UGC5205 to estimate an upper limit on the $\text{H}\alpha$ emission. As above, we fit the N II lines in the vicinity of $\text{H}\alpha$ in addition to $\text{H}\alpha$, $\text{H}\beta$, $\text{H}\gamma$, and $\text{H}\delta$. We fix the equivalent width of $\text{H}\alpha$ to be half that of the other Balmer lines following González Delgado et al. (1999). From this procedure, we estimate an upper limit of $\text{EW}_{\text{H}\alpha} < 3.1 \text{ \AA}$ after correction for stellar absorption and $\text{EW}_{\text{H}\alpha} < 0.35 \text{ \AA}$ if we ignore the absorption correction.

To convert $\text{H}\alpha$ equivalent widths to $\text{H}\alpha$ luminosities, we adapt the method⁵ of Bauer et al. (2013) as follows:

$$\frac{L_{\text{H}\alpha}}{[\text{erg s}^{-1}]} = 3 \times 10^{25} \frac{\text{EW}_{\text{H}\alpha}}{\lambda_{\text{H}\alpha, \text{obs}}} 10^{\frac{M_r - 34.1}{-2.5}} \left(\frac{F_{\text{H}\alpha}/F_{\text{H}\beta}}{2.86} \right)^{2.36}, \quad (3)$$

where our absolute r-band magnitudes are tabulated for each galaxy in Table 2. We note that this method assumes that the equivalent width measured in the central SDSS spectrum is equal to the average equivalent width across the face of the galaxy. Our estimate is therefore likely to be biased high given that the SDSS fiber is placed on the galaxy’s central starburst (we show the placement of the SDSS fiber, as well as the optical spec-

trum of PGC027864, in Appendix A) – as such, the integrated $\text{H}\alpha$ SFR for PGC027864 should be taken only as a rough estimate to demonstrate the galaxy’s star-bursting nature.

Figure 8 shows a comparison of our $\text{H}\alpha$ and UV-based star formation rate estimates, along with a local comparison sample of Local Volume Legacy galaxies (Dale et al. 2023). Here, the filled square symbols show the UV-based SFRs of UGC5205 and PGC027864, while the filled circle (in the case of PGC027864) and the unfilled triangle (for UGC5205) show the $\text{H}\alpha$ -based SFR and upper limit, respectively. Here, one may immediately notice that although the UV-based SFR estimates of UGC5205 and PGC027864 place both galaxies on the SFMS as defined by Dale et al. (2023), there has been a marked divergence in star formation behavior between the ~ 100 Myr timescales probed by UV emission and the ~ 10 Myr timescales probed by $\text{H}\alpha$ emission. While the $\text{H}\alpha$ -based SFR of PGC027864 places the galaxy well above the SFMS in the vigorously star-bursting regime, the $\text{H}\alpha$ non-detection of UGC5205 indicates that star formation has very recently quenched in the galaxy. We will return to this divergence of recent star formation behavior in Section 4.

⁵ In particular, we do not include the effect of stellar absorption, as we have already taken this into account during line fitting, or of redshift, given the proximity of our target galaxies.

3.5. The Stellar Populations of UGC5205

The ionized and neutral gas in UGC5205 show a coordinated story of a recently quenched star formation history. Referring back to [Figure 1](#), we see that the stellar continuum and absorption features are clearly detected in the SDSS spectra. Thus, the star formation history as determined from stellar population synthesis can reveal an independent view into the quenching timescale of the galaxy.

We model the star formation history of UGC5205 based on the four SDSS spectra shown in [Figure 1](#). We utilize *Prospector* ([Johnson & Leja 2017](#); [Leja et al. 2017](#); [Johnson et al. 2021](#)) to fit non-parametric star formation histories independently to the four spectra. Allowing for a flexible and non-parametric star-formation history is crucial to capture the very recent burst and then truncation that defines post-starburst galaxies ([Suess et al. 2022a](#)).

We fix the redshift to the systemic redshift of UGC5205 as measured from the stellar absorption features and assume a Chabrier IMF ([Chabrier 2003](#)). We set a uniform prior on the stellar mass in each spatial region between 10^4 and $10^8 M_\odot$ and a uniform prior on the stellar metallicity from $-2 < \log_{10}(Z/Z_\odot) < 0.2$. We use the [Kriek & Conroy \(2013\)](#) dust law, allowing the power-law slope to vary between -1 and 0.4 and the attenuation to vary between $0 < A_V < 2.5$. We assume young stars are attenuated twice as much as older stars, and fix the shape of the IR SED following the [Draine & Li \(2007\)](#) dust emission templates with $U_{\min} = 1.0$, $\gamma_e = 0.01$, and $q_{\text{PAH}} = 2.0$.⁶ We place a uniform prior on the galaxy’s intrinsic velocity dispersion between $50 < \sigma_v < 300 \text{ km s}^{-1}$. Following [Suess et al. \(2022b\)](#), we include both a spectroscopic jitter term and the *Prospector* pixel outlier model, intended to prevent bad spectral pixels from skewing the output.

The model includes three early time bins ($t_{\text{look-back}} > 2 \text{ Gyr}$) with fixed width, then five bins with uniform stellar mass formed but flexible time edges, such that the model can determine the start and end of star formation, then a final bin with flexible time edges and flexible stellar mass formed to capture any low-level recent star formation; [Suess et al. \(2022a\)](#) show that this model is robust to determine quenching time scales.

The derived star formation histories of each SDSS spectrum, along with an example spectrophotometric fit, are shown in [Figure 9](#). We remind the reader that the three off-body spectra (green, red, and purple in

[Figure 9](#)) are centered on bright young stellar clusters along the stellar tidal tail of UGC5205.

We recover a broadly consistent star formation history from all spectra considered, though we caution against an over-interpretation of the seemingly earlier quenching time of the central spectrum (orange) due to the more complex stellar population filling the central fiber. The SDSS spectra are well-represented by a post-starburst system that underwent a coordinated burst and subsequent quenching event 100-300 Myr ago. This is highly consistent with the picture of a post-starburst system presented in [Figure 8](#), and places a timescale for the quenching event that is independent of the ionized gas emission.

3.6. Neighboring Galaxies

By standard definitions, UGC5205 is considered a field dwarf galaxy in that it is separated by more than 2.5 Mpc and 1000 km s^{-1} from the nearest massive galaxy ([Geha et al. 2012](#)). However, in addition to PGC027864, there are two galaxies in the vicinity of UGC5205, NSA6 and IC0560.

As shown in [Table 2](#), NSA6 is close in stellar mass to UGC5205 and PGC027864. IC0560, with an absolute 2MASS Ks-band magnitude of $M_{K_s} = -22$ ([Skrutskie et al. 2006](#)) and an estimated stellar mass of $1.93 \times 10^{10} M_\odot$, lies just under the cutoff to be considered massive by the [Geha et al. \(2012\)](#) criterion ($M_{K_s} < -23$ or $M_\star > 2.5 \times 10^{10} M_\odot$). These galaxies are selected to be within two projected virial radii of UGC5205 at their redshift and within $\Delta v < 1000 \text{ km s}^{-1}$, though both are significantly offset ($|\Delta v| \sim 300 \text{ km s}^{-1}$) than PGC027864 ($|\Delta v| \sim 50 \text{ km s}^{-1}$) from UGC5205 in line-of-sight velocity.

In [Figure 10](#) we show the position of UGC5205 with respect to these possible neighbor galaxies, where the bold cross indicates UGC5205 and the filled points indicate the three potential neighbors. The large unfilled circles around each filled point indicate the on-sky size of the galaxy’s estimated virial radius at its redshift, where we use the stellar-to-halo mass relation of [Behroozi et al. \(2019\)](#) to make a crude estimate of M_{vir} of each galaxy and estimate its virial radius as

$$R_{\text{vir}} = \left(\frac{M_{\text{vir}}}{\frac{4\pi}{3} 200 \rho_c(z=0)} \right)^{1/3} \quad (4)$$

following [Bryan et al. \(1999\)](#), where ρ_c is the critical density. From this initial estimate, we find that UGC5205 lies within the virial radius of PGC027864 and NSA6, but outside that of IC0560. This separation from IC0560 is especially important given that the star formation behavior of UGC5205 is unusual for a non-satellite galaxy.

⁶ We have also run the fit using $\gamma_e = 0.431$ and $U_{\min} = 4$ based on the values quoted by [Draine & Li \(2007\)](#) for the low-mass galaxies NGC5195 and Mrk33. We find that altering these parameters do not significantly alter our inferred SFHs.

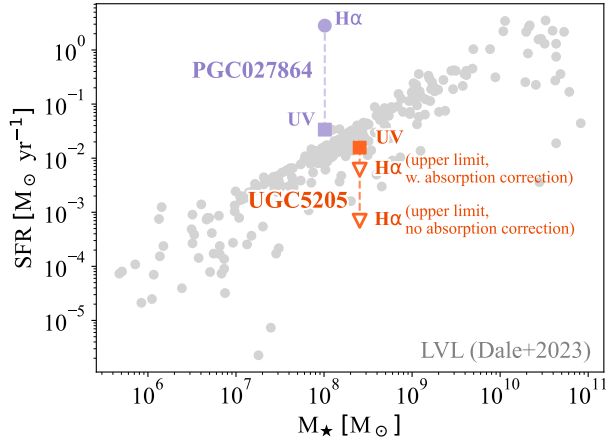


Figure 8. The placement of UGC5205 and PGC027864 relative to the low-mass star-forming main sequence (SFMS) as measured from UV-optical-IR SED fits of Dale et al. (2023). The square symbols show UV-based SFR estimates, while the round circle and unfilled triangle show the $H\alpha$ -based SFR estimate of PGC027864 and the $H\alpha$ upper limit estimate of UGC5205. We find that the UV-based SFR estimates, which reflect SFR over ~ 100 Myr timescales, lie on or near the SFMS for both UGC5205 and PGC027864. The $H\alpha$ -based estimates, however, indicate strongly divergent recent (~ 5 Myr) behavior of UGC5205 and PGC027864 wherein the UGC5205 is quenched and the SFR of PGC027864 has been boosted relative to the SFMS by nearly two orders of magnitude.

As detailed in Appendix C, we find that IC0560 is unable to exert sufficient ram pressure to strip the gas reservoir of UGC5205.

We detail the optical properties of all three galaxies in the vicinity of UGC5205 (and UGC5205 itself) in Table 2. We retrieve redshifts and absolute r-band magnitudes for each galaxy from the NASA Sloan Atlas (Blanton et al. 2011) with the exception of UGC5205, where we remeasure the redshift from the absorption features in the SDSS spectrum placed on the main body of the galaxy. Stellar mass estimates are then made using the g and r -band NSA photometry and with the color-mass relation of Kado-Fong et al. (2022a), which was calibrated against SED-based stellar mass estimates in the dwarf regime.

4. DISCUSSION

Although UGC5205 is only a single galaxy, the existence of a quenched dwarf in the field is significant to our understanding of low-mass galaxy star formation regulation due to their marked rarity at the stellar mass of UGC5205 (Geha et al. 2012). In this discussion, we will consider both how UGC5205 came to be quenched and

Table 2. Optical properties of UGC5205 and nearby galaxies

Galaxy	cz	M_r	R_{proj}	M_\star
	km s^{-1}		kpc	$10^8 M_\odot$
UGC5205	1500	-16.24	–	2.54
NSA 6	1228	-15.27	50.6	1.22
PGC027864	1449	-16.24	9.8	1.02
IC 0560	1848	-19.15	271.0	193

NOTE—The optical properties of UGC5205 and galaxies within two projected virial radii of UGC5205. Redshifts and absolute r-band magnitudes are drawn from the NASA Sloan Atlas except for UGC5205, wherein the redshift was remeasured from optical absorption features in the SDSS spectrum of the main body. The stellar mass of each galaxy was inferred from the relation measured by Kado-Fong et al. (2022a), which was calibrated from galaxies of this stellar mass range.

what implications the existence of a quenched field dwarf has on our understanding of star formation regulation in isolated dwarf galaxies.

4.1. The Quenching Timescale of UGC5205

The combination of a lack of $H\alpha$ emission, a strong UV detection (Section 3.4), and a predominantly young stellar population (Section 3.5) paint a consistent story of a galaxy that underwent a global quenching event ~ 100 – 300 Myr ago.

We can also make a rough, back of the envelope calculation of the lookback time at which the tidal features seen in the HI of UGC5205 were launched based on their extent and velocity relative to the systemic velocity of UGC5205. Due to the complex dynamics of the dwarf interaction, a hydrodynamic simulation would be necessary to truly place a timescale on the merger interaction, but here we can at least make a rough consistency check of the merger-driven quenching picture.

The HI tails B1 and B2 are roughly $56''$ and $72''$ in extent, which corresponds to 5.8 kpc and 7.5 kpc at the distance of UGC5205 assuming an angular diameter distance of $d_A = 21.3$ Mpc based on its recessional velocity of 1500 km s^{-1} . Their mean velocities, as determined by a geometric mean of the moment one map, are 1520 km s^{-1} and 1544 km s^{-1} , respectively. If we simply estimate the creation timescale assuming a constant velocity, we arrive at a launching lookback time of $t_{lb} = 280$ Myr and $t_{lb} = 160$ Myr for B1 and B2 assuming that the transverse velocity is equal to the difference

in velocity between the tidal tail and the systemic stellar velocity of UGC5205. This is consistent with the picture wherein the tidal features were pulled out of the HI reservoir during or shortly after the starburst event, and strengthens the interpretation of a interaction-driven quenching picture for UGC5205.

4.2. HI Properties

Prior to the resolved HI data presented in this work, single dish observations revealed a large reservoir of cold gas associated with UGC5205 (Springob et al. 2005). It was unclear, then, how UGC5205 could support a large reservoir of HI and yet be completely devoid of recent star formation.

The spatially-resolved VLA observations presented in this work show that the bulk of the HI reservoir of UGC5205 is indeed not spatially coincident with the bulk of the stellar mass of the galaxy and has instead been pulled out into two large tidal tails. Furthermore, both tails are offset in velocity from the systemic redshift as measured from stellar absorption features in the same direction. Indeed, the HI morphology of UGC5205 suggests that the lack of recent star formation in the galaxy is borne out of a dearth of cold gas in the galaxy center and not an anomalously low star formation efficiency, as may be suggested from single dish observations alone.

Along these lines, we find that the HI morphology of PGC027864 – the starbursting neighbor of UGC5205 – is relatively undisturbed. With the majority of its cold gas remaining near its center, PGC027864 has much more cold gas available for star formation than UGC5205 despite a similar total HI mass. The difference in the spatial distribution of the cold gas provides a clear explanation for the divergent star formation behavior of UGC5205 and PGC027864. Furthermore, the divergence of morphological and kinematic properties of this dwarf pair – despite their similar global HI properties – underlines the need for interferometric imaging to shed light on the physical processes that shape galaxies’ gas reservoirs.

4.3. Implications for Quenching Dwarfs in the Field

It has been shown that the build-up of a quiescent galaxy population at $M_{\star} \lesssim 10^{8.5} M_{\odot}$ is negligible for non-satellite galaxies. The properties of UGC5205 demonstrate that dwarfs can indeed quench outside of the influence of a massive host for short timescales ($5 \lesssim \tau \lesssim 500$ Myr), while the dearth of a larger population of similar galaxies implies that UGC5205 will not remain quenched.

The spatial distribution of the HI associated with UGC5205 implies that the galaxy has entered a period

of quiescence through its interaction with the nearby dwarf PGC027864. In this section, we will explore the implication of UGC5205’s quenched status on the overall occurrence rate of quenched field galaxies.

4.3.1. Dwarf-Dwarf Mergers

Both projected distance and velocity difference point to a clear ongoing interaction between UGC5205 and PGC027864. Indeed, PGC027864 is currently undergoing a strong starburst; such starbursting periods have been shown to correlate with major mergers between low-mass galaxies (Stierwalt et al. 2015; Privon et al. 2017; Kado-Fong et al. 2020). As shown in Figure 4 and Figure 6, however, there is little evidence to indicate a disturbance in the HI reservoir of PGC027864. This asymmetry in outcomes implies an asymmetry in the pair which allows PGC027864 to retain its HI reservoir while presumably instigating significant tidal disruption in UGC5205, despite their similar stellar masses (see Table 2). Potential asymmetries include highly different mass-to-light ratios (though we note that we have demonstrated that PGC027864 lies on the baryonic Tully-Fisher Relation) or a difference in the concentration of the original HI profile which made UGC5205 relatively more susceptible to stripping.

Regardless of the reason for the asymmetry, however, the existence of UGC5205 shows that interactions between low-mass galaxies may provide a viable way to quench star formation in field dwarfs. The tidal morphology and kinematics of the HI around UGC5205 as well as the coincident starburst and tidal feature creation paint a consistent picture in which the interaction between UGC5205 and PGC027864 both triggered star formation in PGC027864 and quenched star formation in UGC5205.

Finally, as briefly noted in Section 3.2, the gaseous tidal features around UGC5205 remain bound to the galaxy. This means that the cold gas associated with UGC5205 should eventually reaccrete onto the system and reignite star formation. In particular, using the approximate halo properties from Section 3.6 and the halo mass-concentration relation of Child et al. (2018), we estimate a freefall time of

$$t_{ff} = \sqrt{\frac{3\pi}{32G\rho}} \approx 260 \text{ Myr} \quad (5)$$

at the largest point of extent of the HI tidal tails. From our inferred SFH of Section 3.5, UGC5205 has already been quenched for $\lesssim 300$ Myr, implying that the total time that UGC5205 will be quenched by this interaction is $t \lesssim 560$ Myr. We therefore suggest that low-mass

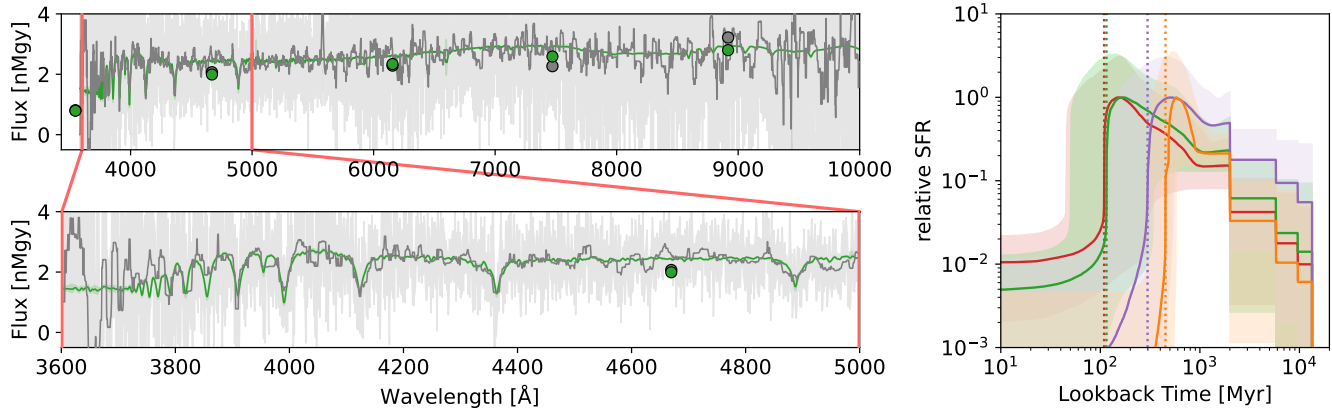


Figure 9. The star formation history of UGC5205 as estimated from stellar population synthesis fits to the SDSS spectra and HSC-SPP photometry shown in Figure 1. At left we show the observed (grey) and model (green) spectra and photometry; the top shows the full spectrophotometric fit, while the bottom shows the Balmer absorption features. The light grey curves show the original SDSS spectrum, while the dark grey curves show the spectrum with a median filter with a kernel size of 15 pixels (median size of 20 Å) applied. At right we show the best-fit SFH for all of the SDSS spectra taken along the tail, with the same color coding as Figure 1. The orange curve shows the SFH derived from the central fiber, while the red, green, and purple curves show the SFH derived from the fibers placed on the stellar tidal tail. The dotted lines show the time at which the SFR dropped to 10% its maximum. We see evidence for a starburst and quenching event between 100-300 Myr ago, consistent with the stark contrast in UV- and H α -inferred star formation rates seen in Figure 8.

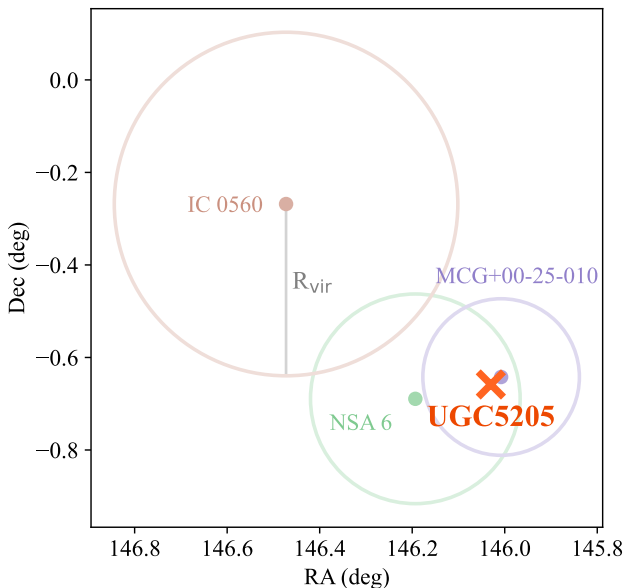


Figure 10. The position of UGC5205 (red cross) compared to nearby galaxies with a velocity difference of $\Delta v < 1000 \text{ km s}^{-1}$ and a projected distance of $R < 2R_{\text{vir}}$. The filled points show the location of each neighboring galaxy; we show the estimated on-sky extent of the virial radius of each galaxy at its redshift by the unfilled circles of the same color. UGC5205 is within R_{vir} of two low-mass galaxies, the $M_r \approx -15$ PGC027864 and $M_r \approx -16$ NSA6, but beyond R_{vir} of the intermediate-mass galaxy IC0560 ($M_r \approx -19$).

interactions such as the system in this work provide an

avenue to *temporarily* quench star formation. Such a mechanism is in good agreement with observations that quenched dwarfs account for, at most, a few percent of low-mass galaxies in the field (Geha et al. 2012).

4.3.2. Low-Mass Group/Filament

Interestingly, UGC5205 is located around 2 Mpc from another quenched field dwarf of stellar mass $M_* \sim 2 \times 10^6 M_\odot$, COSMOS-dw1 (Polzin et al. 2021). The projected distance places these two galaxies a factor of several beyond each other’s virial radii given their velocities, making a direct interaction between the dwarfs highly unlikely. However, the relative proximity of two independently discovered highly rare objects suggests that a larger scale environmental factor may be at play in producing these quenched field dwarfs.

Polzin et al. (2021) suggested internal feedback from star formation to be the mechanism which has temporarily quenched COSMOS-dw1. This interpretation is more feasible for COSMOS-dw1 given that it is a factor of ~ 100 lower in stellar mass than UGC5205, but does not explain why two quenched dwarfs would be found within a few Mpc of each other. Similarly, our interpretation that the interaction with PGC027864 has temporarily quenched UGC5205 connects more directly to the environment of UGC5205 but does not directly imply the existence of another quenched dwarf at a separation larger than several virial radii.

The moderate spatial proximity of these two quenched systems is especially puzzling given that UGC5205

has been identified as a void galaxy (Pustilnik et al. 2019). This makes it difficult to envision a scenario in which a large-scale cosmic filament would be responsible for quenching both UGC5205 and COSMOS-dw1. However, we note that the void catalog of Pustilnik et al. (2019) was constructed using only those galaxies brighter than $M_K = -22$; it is thus possible that UGC5205 and COSMOS-dw1 are connected by a large-scale structure traced only by low-mass galaxies. At this point, an attempt to define such a structure based on the existence of UGC5205 and COSMOS-dw1 would be highly speculative. A further spectroscopic exploration of other low-mass galaxies in the vicinity of these two quenched field dwarfs will be necessary to more conclusively establish a link between the unusual quenched nature of these two galaxies.

5. CONCLUSIONS

In this work we have presented new spatially resolved HI observations of the interacting field dwarf system UGC5205 and PGC027864. Despite the fact that they are remarkably similar in their integrated UV, optical, and HI properties, one dwarf is quenched ($EW_{H\alpha} < 2 \text{ \AA}$) and the other is starbursting ($EW_{H\alpha} > 1000 \text{ \AA}$) in this peculiar pair. The existence of UGC5205, a quenched dwarf in the field, is intriguing due to the fact that the quiescent field dwarf population is still poorly understood at this stellar mass. Previous works have put an upper limit on the quenched fraction at the stellar mass of UGC5205, but this galaxy represents a novel opportunity to directly understand the nature of quenching processes at this mass scale.

With our new VLA observations, we have shown that:

- Approximately half of the HI reservoir of UGC5205 has been pulled into large tidal tails that are spatially and kinematically offset from the main stellar body of UGC5205, making most of the cold gas in the galaxy unavailable for star formation despite a sizable total HI mass.
- The HI reservoir of PGC027864, conversely, shows only minor disturbance. The core can be fit by a tilted ring model, with some emission from tidal HI visible along the axis of the dwarf pair.

This asymmetry in HI morphology provides a clear explanation for the marked divergence in the apparent global star formation efficiency (defined simply as SFR/M_{HI}) of UGC5205 and PGC027864.

With this morphological information in hand, and given the lack of other likely disrupting bodies, we suggest that it is the ongoing interaction with PGC027864

that has temporarily quenched UGC5205. This interpretation is supported by the fact that the timing of the quenching event in UGC5205, as inferred both by the UV and $H\alpha$ emission (or lack thereof, Section 3.4) and from stellar population fitting of UGC5205 (Section 3.5), is coincident with the rough lookback time at which the gaseous tidal features were created (Section 4.1) Under this assertion, we can examine the implications of UGC5205 on the build-up of a population of quenched dwarfs:

- UGC5205 and PGC027864 show that dwarf-dwarf interactions are not only able to trigger starbursts, but also quench star formation. Both phenomena can moreover happen simultaneously in the same interaction.
- Given that the HI in UGC5205 likely remains bound to the system, the sizable cold gas reservoir should eventually reaccrete and reignite star formation in the system. Based off our inferred SFH and an estimate of the freefall time at the position of the tidal features, we estimate a total quenched period of $\approx 560 \text{ Myr}$. This suggests that interaction-driven quenching events are temporary in low-mass systems.
- UGC5205 is 2 Mpc away from the lower mass quenched field dwarf COSMOS-dw1. Given their low masses, this distance is too far for a direct interaction between the quenched dwarfs. Furthermore, while UGC5205 is highly consistent with a pair interaction quenching picture, COSMOS-dw1 has been suggested to have self-quenched through star formation feedback. However, it is possible that a large-scale structure populated by low-mass objects could increase the efficacy of both quenching mechanisms.

The dwarf pair demonstrates that the star formation behavior of low-mass galaxies is sensitive not only to the presence of massive host galaxies, as has been studied in depth in the literature (see, e.g. Geha et al. 2012, 2017; Carlsten et al. 2020, 2021; Mao et al. 2021; Carlsten et al. 2022), but also to the presence of other low-mass galaxies, which has previously been explored only in the enhanced star formation scenario (see, e.g. Stierwalt et al. 2015; Pearson et al. 2016; Privon et al. 2017; Kado-Fong et al. 2020; Subramanian et al. 2023).

The existence of UGC5205 and its low-mass neighbors demonstrate the potential of a new avenue for understanding star formation regulation in dwarf galaxies outside the influence of a massive host. Characterizing just one of these rare quiescent field dwarfs has shed

new light on the role of low-mass interactions in regulating dwarf star formation – assembling a larger sample of quenched field dwarfs would provide even more novel constraints on the duty cycle and efficiency of such quenching events. TiNy Titans has established a sample of dwarf multiples for galaxies with SDSS spectroscopy; the upcoming generation of deeper surveys will, on timescales within a few years, push this pair-finding out to larger volumes and lower masses (Darragh-Ford et al. 2022; Luo et al. 2023) and shed new light into the regulation and evolution of star formation in low-mass galaxies.

The authors thank George Privon for helpful conversations that improved the quality of this manuscript. The authors also thank the anonymous referee for their insightful comments that improved the quality of this work.

EKF gratefully acknowledges support from the Yale Center for Astronomy and Astrophysics Prize Postdoctoral Fellowship.

The National Radio Astronomy Observatory is a facility of the National Science Foundation operated under cooperative agreement by Associated Universities, Inc.

Basic research in radio astronomy at the U.S. Naval Research Laboratory is supported by 6.1 Base Funding.

The Hyper Suprime-Cam (HSC) collaboration includes the astronomical communities of Japan and Taiwan, and Princeton University. The HSC instrumentation and software were developed by the National Astronomical Observatory of Japan (NAOJ), the Kavli Institute for the Physics and Mathematics of the Universe (Kavli IPMU), the University of Tokyo, the High Energy Accelerator Research Organization (KEK), the Academia Sinica Institute for Astronomy and Astrophysics in Taiwan (ASIAA), and Princeton University. Funding was contributed by the FIRST program from the Japanese Cabinet Office, the Ministry of Education, Culture, Sports, Science and Technology (MEXT), the Japan Society for the Promotion of Science (JSPS), Japan Science and Technology Agency (JST), the Toray Science Foundation, NAOJ, Kavli IPMU, KEK, ASIAA, and Princeton University.

This paper makes use of software developed for Vera C. Rubin Observatory. We thank the Rubin Observatory for making their code available as free software at <http://pipelines.lsst.io/>.

This paper is based on data collected at the Subaru Telescope and retrieved from the HSC data archive system, which is operated by the Subaru Telescope and Astronomy Data Center (ADC) at NAOJ. Data analysis was in part carried out with the cooperation of Center for Computational Astrophysics (CfCA), NAOJ. We are honored and grateful for the opportunity of observing the Universe from Maunakea, which has the cultural, historical and natural significance in Hawaii.

Based on observations made with the NASA Galaxy Evolution Explorer. GALEX is operated for NASA by the California Institute of Technology under NASA contract NAS5-98034.

Funding for the SDSS and SDSS-II has been provided by the Alfred P. Sloan Foundation, the Participating Institutions, the National Science Foundation, the U.S. Department of Energy, the National Aeronautics and Space Administration, the Japanese Monbukagakusho, the Max Planck Society, and the Higher Education Funding Council for England. The SDSS Web Site is <http://www.sdss.org/>. The SDSS is managed by the Astrophysical Research Consortium for the Participating Institutions. The Participating Institutions are the American Museum of Natural History, Astrophysical Institute Potsdam, University of Basel, University of Cambridge, Case Western Reserve University, University of Chicago, Drexel University, Fermilab, the Institute for Advanced Study, the Japan Participation Group, Johns Hopkins University, the Joint Institute for Nuclear Astrophysics, the Kavli Institute for Particle Astrophysics and Cosmology, the Korean Scientist Group, the Chinese Academy of Sciences (LAMOST), Los Alamos National Laboratory, the Max-Planck-Institute for Astronomy (MPIA), the Max-Planck-Institute for Astrophysics (MPA), New Mexico State University, Ohio State University, University of Pittsburgh, University of Portsmouth, Princeton University, the United States Naval Observatory, and the University of Washington.

REFERENCES

- Bauer, A. E., Hopkins, A. M., Gunawardhana, M., et al. 2013, *MNRAS*, 434, 209, doi: [10.1093/mnras/stt1011](https://doi.org/10.1093/mnras/stt1011)
- Behroozi, P., Wechsler, R. H., Hearin, A. P., & Conroy, C. 2019, *MNRAS*, 488, 3143, doi: [10.1093/mnras/stz1182](https://doi.org/10.1093/mnras/stz1182)
- Bertin, E., & Arnouts, S. 1996, *A&AS*, 117, 393, doi: [10.1051/aas:1996164](https://doi.org/10.1051/aas:1996164)
- Besla, G., Patton, D. R., Stierwalt, S., et al. 2018, *MNRAS*, 480, 3376, doi: [10.1093/mnras/sty2041](https://doi.org/10.1093/mnras/sty2041)
- Blanton, M. R., Kazin, E., Muna, D., Weaver, B. A., & Price-Whelan, A. 2011, *AJ*, 142, 31, doi: [10.1088/0004-6256/142/1/31](https://doi.org/10.1088/0004-6256/142/1/31)

- Blanton, M. R., & Moustakas, J. 2009, *ARA&A*, 47, 159, doi: [10.1146/annurev-astro-082708-101734](https://doi.org/10.1146/annurev-astro-082708-101734)
- Bryan, G. L., Machacek, M., Anninos, P., & Norman, M. L. 1999, *ApJ*, 517, 13, doi: [10.1086/307173](https://doi.org/10.1086/307173)
- Carlsten, S. G., Greco, J. P., Beaton, R. L., & Greene, J. E. 2020, *ApJ*, 891, 144, doi: [10.3847/1538-4357/ab7758](https://doi.org/10.3847/1538-4357/ab7758)
- Carlsten, S. G., Greene, J. E., Beaton, R. L., Danieli, S., & Greco, J. P. 2022, *ApJ*, 933, 47, doi: [10.3847/1538-4357/ac6fd7](https://doi.org/10.3847/1538-4357/ac6fd7)
- Carlsten, S. G., Greene, J. E., Greco, J. P., Beaton, R. L., & Kado-Fong, E. 2021, *ApJ*, 922, 267, doi: [10.3847/1538-4357/ac2581](https://doi.org/10.3847/1538-4357/ac2581)
- CASA Team, Bean, B., Bhatnagar, S., et al. 2022, *PASP*, 134, 114501, doi: [10.1088/1538-3873/ac9642](https://doi.org/10.1088/1538-3873/ac9642)
- Chabrier, G. 2003, *PASP*, 115, 763, doi: [10.1086/376392](https://doi.org/10.1086/376392)
- Child, H. L., Habib, S., Heitmann, K., et al. 2018, *ApJ*, 859, 55, doi: [10.3847/1538-4357/aabf95](https://doi.org/10.3847/1538-4357/aabf95)
- Conroy, C., & Gunn, J. E. 2010, *ApJ*, 712, 833, doi: [10.1088/0004-637X/712/2/833](https://doi.org/10.1088/0004-637X/712/2/833)
- Dale, D. A., Boquien, M., Turner, J. A., et al. 2023, *AJ*, 165, 260, doi: [10.3847/1538-3881/accffe](https://doi.org/10.3847/1538-3881/accffe)
- Darragh-Ford, E., Wu, J. F., Mao, Y.-Y., et al. 2022, *arXiv e-prints*, arXiv:2212.07433, doi: [10.48550/arXiv.2212.07433](https://doi.org/10.48550/arXiv.2212.07433)
- Di Teodoro, E. M., & Fraternali, F. 2015, *MNRAS*, 451, 3021, doi: [10.1093/mnras/stv1213](https://doi.org/10.1093/mnras/stv1213)
- Draine, B. T., & Li, A. 2007, *ApJ*, 657, 810, doi: [10.1086/511055](https://doi.org/10.1086/511055)
- Eldridge, J. J., & Stanway, E. R. 2016, *MNRAS*, 462, 3302, doi: [10.1093/mnras/stw1772](https://doi.org/10.1093/mnras/stw1772)
- Geha, M., Blanton, M. R., Yan, R., & Tinker, J. L. 2012, *ApJ*, 757, 85, doi: [10.1088/0004-637X/757/1/85](https://doi.org/10.1088/0004-637X/757/1/85)
- Geha, M., Wechsler, R. H., Mao, Y.-Y., et al. 2017, *ApJ*, 847, 4, doi: [10.3847/1538-4357/aa8626](https://doi.org/10.3847/1538-4357/aa8626)
- González Delgado, R. M., Leitherer, C., & Heckman, T. M. 1999, *ApJS*, 125, 489, doi: [10.1086/313285](https://doi.org/10.1086/313285)
- Gunn, J. E., & Gott, J. Richard, I. 1972, *ApJ*, 176, 1, doi: [10.1086/151605](https://doi.org/10.1086/151605)
- Hopkins, P. F., Hernquist, L., Cox, T. J., & Kereš, D. 2008, *ApJS*, 175, 356, doi: [10.1086/524362](https://doi.org/10.1086/524362)
- Izotov, Y. I., & Thuan, T. X. 2016, *MNRAS*, 457, 64, doi: [10.1093/mnras/stv2957](https://doi.org/10.1093/mnras/stv2957)
- Johnson, B., & Leja, J. 2017, *bd-j/prospector: Initial release, v0.1*, Zenodo, Zenodo, doi: [10.5281/zenodo.1116491](https://doi.org/10.5281/zenodo.1116491)
- Johnson, B. D., Leja, J., Conroy, C., & Speagle, J. S. 2021, *ApJS*, 254, 22, doi: [10.3847/1538-4365/abef67](https://doi.org/10.3847/1538-4365/abef67)
- Kado-Fong, E., Greene, J. E., Huang, S., et al. 2020, *ApJ*, 900, 163, doi: [10.3847/1538-4357/abacc2](https://doi.org/10.3847/1538-4357/abacc2)
- Kado-Fong, E., Greene, J. E., Huang, S., & Goulding, A. 2022a, *ApJ*, 941, 11, doi: [10.3847/1538-4357/ac9964](https://doi.org/10.3847/1538-4357/ac9964)
- Kado-Fong, E., Kim, C.-G., Greene, J. E., & Lancaster, L. 2022b, *ApJ*, 939, 101, doi: [10.3847/1538-4357/ac9673](https://doi.org/10.3847/1538-4357/ac9673)
- Kennicutt, Jr., R. C. 1998, *ARA&A*, 36, 189, doi: [10.1146/annurev.astro.36.1.189](https://doi.org/10.1146/annurev.astro.36.1.189)
- Koribalski, B. S., Staveley-Smith, L., Kilborn, V. A., et al. 2004, *AJ*, 128, 16, doi: [10.1086/421744](https://doi.org/10.1086/421744)
- Kriek, M., & Conroy, C. 2013, *ApJL*, 775, L16, doi: [10.1088/2041-8205/775/1/L16](https://doi.org/10.1088/2041-8205/775/1/L16)
- Kroupa, P. 2001, *MNRAS*, 322, 231, doi: [10.1046/j.1365-8711.2001.04022.x](https://doi.org/10.1046/j.1365-8711.2001.04022.x)
- Leja, J., Johnson, B. D., Conroy, C., van Dokkum, P. G., & Byler, N. 2017, *ApJ*, 837, 170, doi: [10.3847/1538-4357/aa5ffe](https://doi.org/10.3847/1538-4357/aa5ffe)
- Leroy, A. K., Walter, F., Brinks, E., et al. 2008, *AJ*, 136, 2782, doi: [10.1088/0004-6256/136/6/2782](https://doi.org/10.1088/0004-6256/136/6/2782)
- Luo, Y., Leauthaud, A., Greene, J., et al. 2023, *arXiv e-prints*, arXiv:2305.19310, doi: [10.48550/arXiv.2305.19310](https://doi.org/10.48550/arXiv.2305.19310)
- Mao, Y.-Y., Geha, M., Wechsler, R. H., et al. 2021, *ApJ*, 907, 85, doi: [10.3847/1538-4357/abce58](https://doi.org/10.3847/1538-4357/abce58)
- Oppenheimer, B. D., Crain, R. A., Schaye, J., et al. 2016, *MNRAS*, 460, 2157, doi: [10.1093/mnras/stw1066](https://doi.org/10.1093/mnras/stw1066)
- Pearson, S., Besla, G., Putman, M. E., et al. 2016, *MNRAS*, 459, 1827, doi: [10.1093/mnras/stw757](https://doi.org/10.1093/mnras/stw757)
- Polzin, A., van Dokkum, P., Danieli, S., Greco, J. P., & Romanowsky, A. J. 2021, *ApJL*, 914, L23, doi: [10.3847/2041-8213/ac024f](https://doi.org/10.3847/2041-8213/ac024f)
- Ponomareva, A. A., Muladzi, W., Maddox, N., et al. 2021, *MNRAS*, 508, 1195, doi: [10.1093/mnras/stab2654](https://doi.org/10.1093/mnras/stab2654)
- Pracy, M. B., Owers, M. S., Couch, W. J., et al. 2012, *MNRAS*, 420, 2232, doi: [10.1111/j.1365-2966.2011.20188.x](https://doi.org/10.1111/j.1365-2966.2011.20188.x)
- Privon, G. C., Stierwalt, S., Patton, D. R., et al. 2017, *ApJ*, 846, 74, doi: [10.3847/1538-4357/aa8560](https://doi.org/10.3847/1538-4357/aa8560)
- Pustilnik, S. A., Tepliakova, A. L., & Makarov, D. I. 2019, *MNRAS*, 482, 4329, doi: [10.1093/mnras/sty2947](https://doi.org/10.1093/mnras/sty2947)
- Quai, S., Hani, M. H., Ellison, S. L., Patton, D. R., & Woo, J. 2021, *MNRAS*, 504, 1888, doi: [10.1093/mnras/stab988](https://doi.org/10.1093/mnras/stab988)
- Schlafly, E. F., & Finkbeiner, D. P. 2011, *ApJ*, 737, 103, doi: [10.1088/0004-637X/737/2/103](https://doi.org/10.1088/0004-637X/737/2/103)
- Senchyna, P., Stark, D. P., Vidal-García, A., et al. 2017, *MNRAS*, 472, 2608, doi: [10.1093/mnras/stx2059](https://doi.org/10.1093/mnras/stx2059)
- Senchyna, P., Stark, D. P., Charlot, S., et al. 2022, *ApJ*, 930, 105, doi: [10.3847/1538-4357/ac5d38](https://doi.org/10.3847/1538-4357/ac5d38)
- Shirazi, M., & Brinchmann, J. 2012, *MNRAS*, 421, 1043, doi: [10.1111/j.1365-2966.2012.20439.x](https://doi.org/10.1111/j.1365-2966.2012.20439.x)
- Skrutskie, M. F., Cutri, R. M., Stiening, R., et al. 2006, *AJ*, 131, 1163, doi: [10.1086/498708](https://doi.org/10.1086/498708)

- Somerville, R. S., Hopkins, P. F., Cox, T. J., Robertson, B. E., & Hernquist, L. 2008, MNRAS, 391, 481, doi: [10.1111/j.1365-2966.2008.13805.x](https://doi.org/10.1111/j.1365-2966.2008.13805.x)
- Springob, C. M., Haynes, M. P., Giovanelli, R., & Kent, B. R. 2005, ApJS, 160, 149, doi: [10.1086/431550](https://doi.org/10.1086/431550)
- Stierwalt, S., Besla, G., Patton, D., et al. 2015, ApJ, 805, 2, doi: [10.1088/0004-637X/805/1/2](https://doi.org/10.1088/0004-637X/805/1/2)
- Stierwalt, S., Liss, S. E., Johnson, K. E., et al. 2017, Nature Astronomy, 1, 0025, doi: [10.1038/s41550-016-0025](https://doi.org/10.1038/s41550-016-0025)
- Subramanian, S., Mondal, C., & Kalari, V. 2023, arXiv e-prints, arXiv:2310.02595, doi: [10.48550/arXiv.2310.02595](https://doi.org/10.48550/arXiv.2310.02595)
- Suess, K. A., Leja, J., Johnson, B. D., et al. 2022a, ApJ, 935, 146, doi: [10.3847/1538-4357/ac82b0](https://doi.org/10.3847/1538-4357/ac82b0)
- Suess, K. A., Kriek, M., Bezanson, R., et al. 2022b, ApJ, 926, 89, doi: [10.3847/1538-4357/ac404a](https://doi.org/10.3847/1538-4357/ac404a)

APPENDIX

A. SDSS SPECTRUM OF PGC027864

In addition to the four spectra taken of UGC5205, there is one SDSS spectrum associated with the companion PGC027864. In [Figure 11](#), we show this spectrum and its placement with respect to the galaxy; unlike UGC5205, the optical spectrum shows strong line emission that indicates that PGC027864 is actively starbursting.

As in the analogous main text figure ([Figure 1](#)), at left we show a *gri*-composite image of the UGC5205 and PGC027864 system with the position of the SDSS fiber on PGC027864 overlaid. The inner circle shows the on-sky size of the 3" diameter fiber. At right we show the spectrum itself; unlike [Figure 1](#), we do not show a binned version of the spectrum due to the high SNR of the emission lines.

B. ANCILLARY HI DATA

B.1. *Archival HI Observations*

Single dish observations of UGC5205 and PGC027864 find a gas-rich system. [Figure 12](#) shows HI line profiles from the HI Parkes All Sky Survey (HIPASS, [Koribalski et al. 2004](#)) and Arecibo ([Springob et al. 2005](#)). The HIPASS beam contains both UGC5205 and PGC027864, while the Arecibo beam is centered on UGC5205 and grazes the southwestern edge of PGC027864. The HIPASS HI profile shows a peak at the redshift of PGC027864; this gas is likely the origin of the asymmetric tail in the Springob et al. (2005) line profile, as the Arecibo beam includes a part of PGC027864. The main peak of the HI profiles, however, is shifted redwards of UGC5205, as is seen in the spatially resolved VLA data.

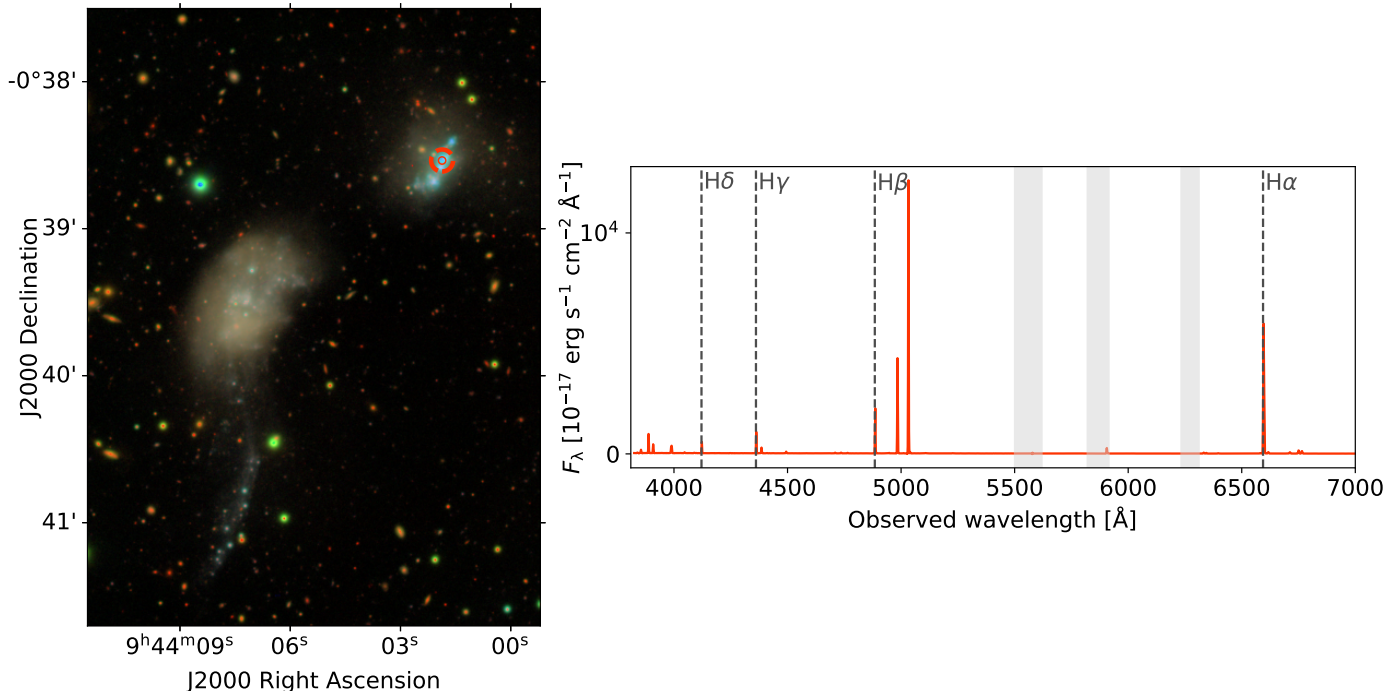


Figure 11. The same as [Figure 1](#), but showing the SDSS spectra associated with the companion PGC027864. Unlike UGC5205, strong line emission is clearly present in the central spectrum of PGC027864.

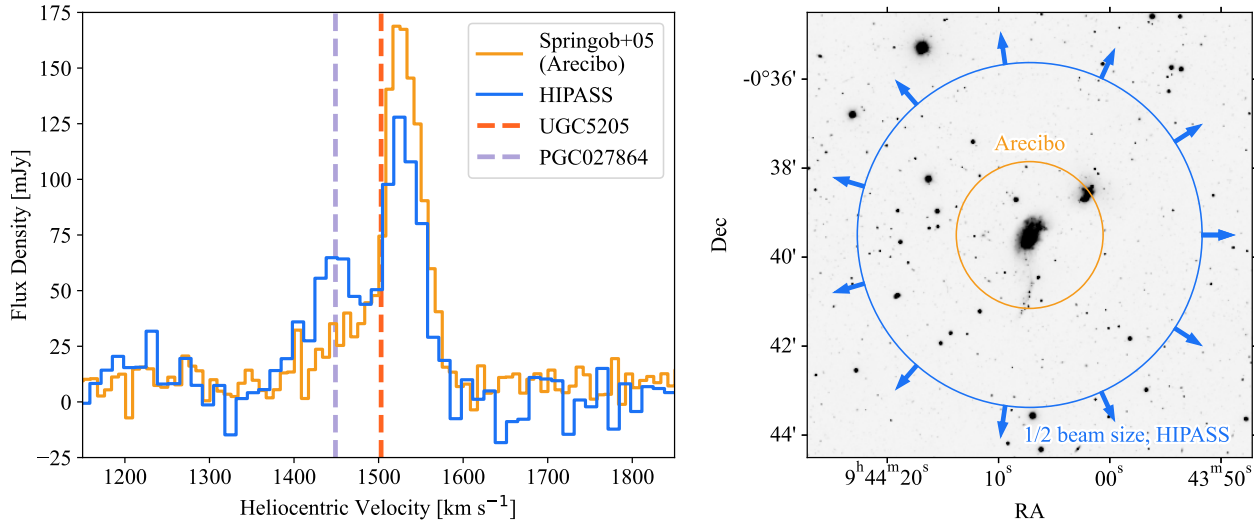


Figure 12. The 21cm-line spectra (left) and approximate spatial extent (right) of the archival HI observations of HIPASS and Springob et al. (2005) centered on UGC5205. At left, we also overlay the mean heliocentric velocity of UGC5205 and PGC027864 as dashed orange and purple vertical lines, respectively. The Arecibo beam (HPBW= 3.3 arcmin) covers all of UGC5205 and part of PGC027864, as shown on the right. The HIPASS beam (gridded beamsize of 15.5 arcmin) covers both galaxies; in the right panel, the HIPASS beam extends beyond the figure extent and so for illustrative purposes we plot the aperture equivalent to half the HIPASS beam.

B.2. Integrated Spectra

In order to understand whether we are missing significant flux at spatial scales larger than what can be probed by the high-resolution C-array data, the system was also observed in the D configuration. We show the moment zero map of the D-array data in Figure 13. Much of the spatial structure of the system’s HI (and in particular the disturbed HI associated both with UGC5205 and with PGC027864) is not observed in the D-array data due to the larger beamsize.

To understand whether there is significant 21 cm emission from HI at larger spatial scales than can be reached by the C configuration data, we integrate the spectrum coincident with UGC5205 in both the C-array and D-array data. We extract all the flux from within the black circle shown in Figure 4. The black circle is centered on (09:44:07.714, -03.39.54.389) in order to encompass all of the emission associated with UGC5205 while excluding emission from its nearby companion PGC027864. We find a very good agreement in total flux F between the two integrated spectra, with a fractional difference of $\Delta F/F = 0.26$ for all emission at $\Delta F/F = 0.10$ for gas at $v > 1500 \text{ km s}^{-1}$. There is an excess at velocities of 1400 to 1500 km s^{-1} ; this is at the velocity of PGC027864, and is likely due to some gas associated with the companion contaminating the low resolution D-array data, but not higher resolution the C-array data.

C. THE PLAUSIBILITY OF RAM PRESSURE STRIPPING BY IC0560

Given the singular nature of its current star formation and HI reservoir, we will consider the potential influence of the nearby intermediate-mass galaxy IC0560 on the structure and evolution of UGC5205.

Although UGC5205 is considered a field galaxy by standard methods to determine low-mass galaxy environment (Geha et al. 2012), the intermediate-mass galaxy IC0560 is at a velocity difference of $\Delta v = 550 \text{ km s}^{-1}$. We should thus examine whether this more massive galaxy is able to exert sufficient ram pressure to strip the atomic gas from UGC5205.

Following Gunn & Gott (1972), we define the ram pressure at the position of UGC5205 as

$$P_e = \rho(R_t)\Delta v^2, \quad (\text{C1})$$

where $\rho(r)$ is the (radial) density profile of the circumgalactic medium of IC0560. R_t here is the radial distance of UGC5205 where the center of IC0560 is $R = 0$. The velocity difference $\Delta v = 550 \text{ km s}^{-1}$ here refers to the velocity difference between UGC5205 and IC0560 assuming that both galaxies are at the distance of IC0560.

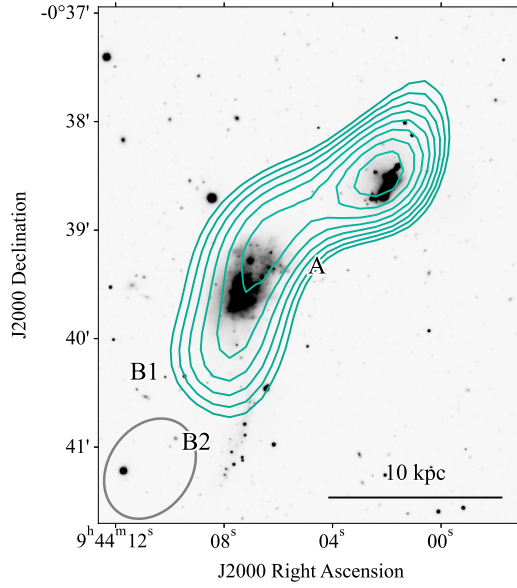


Figure 13. The same as Figure 2 for the moment 0 map of the D-array. Again, the VLA data (teal contours) overlaid over HSC-SSP g-band imaging. The average beamsize of the cube over which the moment 0 map was computed is shown in the bottom left of each panel.

Assuming plane-parallel geometry, the confining weight that the gas feels can be written as:

$$\mathcal{W} = 2\pi G \Sigma_{\star} \Sigma_g, \quad (\text{C2})$$

where Σ_{\star} and Σ_g are the stellar and gas surface densities, respectively. The original treatment of Gunn & Gott (1972) implicitly assumes that the contribution to the weight from dark matter is negligible compared to that from stars – while this may not be true in detail for UGC5205 due to its lower stellar mass, including the effect of dark matter would make the gas even harder to strip than in this simple exercise.

For the hot gas associated with IC0560 to successfully strip the gas from UGC5205, the ram pressure must overcome the external weight felt by the gas. Taking the NASA Sloan Atlas (NSA) photometry of UGC5205, we arrive at an average stellar mass surface density of $\Sigma_{\star} = 40 M_{\odot} \text{ kpc}^{-2}$. The relevant gas surface density differs from the present-day HI surface density for two reasons. First, the relevant distribution of the gas reservoir is the distribution *before* the galaxy’s reservoir was disturbed. Second, our HI observations account for only one phase of the galaxy’s interstellar medium, while this exercise concerns the total gas surface density.

In order to estimate the total, pre-disturbed gas surface density, let us assume that the HI of UGC5205 was originally distributed with the same profile as the present-day stars, but with a scale radius equal to twice that of the half-light radius ($R_{1/2,\star} = 1.9 \text{ kpc}$). We will neglect the dynamical contribution of other phases of the ISM (notably neglecting molecular hydrogen) both because H_2 is likely to play only a minor dynamical role in low-mass galaxies (Leroy et al. 2008; Kado-Fong et al. 2022a) and because neglecting the contribution of H_2 will lead to an underestimate in the IC0560 gas density needed to strip the gas from UGC5205 (i.e., we will over-estimate the capacity for IC0560 to strip UGC5205).

These assumptions lead to average estimated gas surface density of $\Sigma_g = 27 M_{\odot} \text{ pc}^{-2}$. We thus find that for stripping to occur the density of the gas associated with IC0560 at the position of UGC5205 must exceed

$$\begin{aligned} n_H(R_t) &> \frac{2\pi G \Sigma_{\star} \Sigma_g}{m_H \Delta v^2} \\ &> 0.004 \text{ cm}^{-3}. \end{aligned} \quad (\text{C3})$$

Although simulations predict that the circumgalactic medium (CGM) of sub-L* galaxies can exceed this requirement, such densities are only predicted very nearby the galaxy ($R \lesssim 0.1 R_{\text{vir}}$, Oppenheimer et al. 2016). At the present-day

distance of UGC5205, CGM densities of sub- L^* galaxies are several orders of magnitude below this stripping threshold ($n_H \sim 10^{-5} \text{ cm}^{-3}$ at $R = R_{\text{vir}}$). We thus conclude that the disturbed nature of the HI of UGC5205 is not due to ram pressure stripping from gas associated with IC0560.